*Journal of Enzyme Inhibition and Medicinal Chemistry*, 2009; 24(4): 1045–1055

informa
healthcare

**RESEARCH ARTICLE**

# Update on biochemical properties of recombinant *Pseudomonas diminuta* phosphotriesterase

Eugénie Carletti[1], Lilian Jacquamet[2], Mélanie Loiodice[1], Daniel Rochu[1], Patrick Masson[1], and Florian Nachon[1]

[1]*Unité d'Enzymologie, Département de Toxicologie, Centre de Recherches du Service de Santé des Armées (CRSSA), 24 av des Maquis du Grésivaudan, 38700 La Tronche, France, and* [2]*Laboratoire de Cristallogenèse et Cristallographie des Protéines. Institut de Biologie Structurale (CEA-CNRS-UJF), 41 rue Jules Horowitz, 38027 Grenoble, France*



**Abstract**

Phosphotriesterase from *Pseudomonas diminuta* (PTE; EC 3.1.8.1) hydrolyzes organophosphate insecticides and chemical warfare agents. The two zinc cations in the active center can be substituted. $Co^{2+}$-containing PTE is the most efficient but least stable isoform. Gel filtration showed that PTE is monomeric at the submicromolar concentrations used in kinetic assays. The analysis of the recombinant enzyme by X-ray fluorescence spectrometry and CCT-ICP-MS, confirms that recombinant Zn-PTE contains only $Zn^{2+}$ whereas Co-PTE has $Zn^{2+}$ and $Co^{2+}$ in equimolar amount, with $Co^{2+}$ most likely in the reported labile β-site. We noted that recombinant PTE is unstable at low concentrations and must be stabilized by a protein environment. We tested the effect of excess of various metal cofactors on PTE-catalyzed hydrolysis of paraoxon. We notably observed that $ZnCl_2$ induces a non-competitive partial inhibition of $Zn^{2+}$- and $Co^{2+}$-PTE at pH 8.5 (apparent Ki = 155 μM and 52 μM, respectively). Inhibition results from interactions with colloidal $Zn(OH)_2$ formed in alkaline buffer that alters the catalytic machinery. $NiCl_2$ caused a similar effect at higher concentrations (apparent Ki = 3 mM). We observed that mutating His123, a surface residue close to an alleged allosteric site, dramatically altered the bacterial expression yield of $Co^{2+}$-PTE, Ki for $Zn(OH)_2$ inhibition, $k_{cat}$ (up to 60 fold) for paraoxon hydrolysis, but not $K_M$. Issues addressed in this work are important for future biotechnological developments of PTE as a detoxifying enzyme.

**Keywords:** *Phosphotriesterase; organophosphate ester; X-ray fluorescence; non competitive inhibition; colloid*

**Abbreviations:** BSA, Bovine Serum Albumin; CCT-ICP-MS, Collision-reaction Cell Technology - Inductively Coupled plasma - Mass Spectrometry; DEAE, Di-Ethyl-Amino-ethane; EDTA, Ethylene diamine tetra acetic acid; EPN, O-ethyl-O-p-nitrophenyl phenylphosphonothioate; IPTG, Isopropyl β-D-thiogalactopyranoside; KOD, Kodakaraensis; OP, Organophosphate; PCR, Polymerase Chain Reaction; PTE, Phosphotriesterase; PTE*m*, mature Phosphotriesterase; SDS-PAGE, Sodium dodecylsulfate-polyacrylamide gel electrophoresis

## Introduction

Phosphotriesterase (PTE; EC 3.1.8.1) is a member of the amidohydrolase superfamily of enzymes. It was isolated from *Pseudomonas diminuta*. PTE and other organophosphate degrading enzymes: This enzyme became the focus of intense scrutiny because of its demonstrated utility for detoxification of poisonous phosphotriesters, including agricultural pesticides and chemical warfare agents like tabun, sarin, soman and VX [1, 2]. No natural substrate has yet been identified [3] but PTE is suspected to have evolved from a bacterial lactonase [4].

The high-resolution X-ray crystal structure of PTE reveals a homodimeric protein with a single active site with the two $Zn^{2+}$ ions embedded within a $(\beta/\alpha)8$-barrel motif [5]. The two metal ions are bridged by a carboxylated Lys-169 and a hydroxyl ion at neutral pH [6]. The α-$Zn^{2+}$, more buried, is pentacoordinated to His-55, His-57, Asp-301, carboxylated Lys-169 and the hydroxide. The β-$Zn^{2+}$, more solvent-exposed and labile, is pentacoordinated to His-201, His-230, carboxylated Lys-169, the hydroxide and a water molecule. The β-$Zn^{2+}$ is in a distorted trigonal bispyramidal arrangement.

*Address for Correspondence*: Dr. Florian Nachon, Unité d'enzymologie, Département de Toxicologie, Centre de Recherches du Service de Santé des Armées (CRSSA), 24 av des Maquis du Grésivaudan, 38700 La Tronche, France. Tel: +33476639765 / Fax: +33476636962. E-mail: fnachon@crssa.net

*(Received 16 June 2008; revised 02 October 2008; accepted 21 October 2008)*

ISSN 1475-6366 print/ISSN 1475-6374 online © 2009 Informa UK Ltd
DOI: 10.1080/14756360802608518

A comprehensive mechanism for the hydrolysis of phosphotriester by PTE was recently proposed [7]. According to this mechanism, the phosphotriester bond is cleaved in a $SN_2$-like reaction involving a water molecule terminally bound to the α-metal ion. The pKa of this water molecule is lowered though its interaction with the α-metal ion and the bridging hydroxide, generating a hydroxide nucleophile that is ideally aligned to attack the electrophilic phosphorus. This enzyme has a high turnover with OPs as substrates. For example, $k_{cat}$ and $k_{cat}/K_m$ values for the hydrolysis of paraoxon (Scheme 1) approach $10^4$ $s^{-1}$ and $10^8$ $M^{-1}s^{-1}$, respectively [6].

Because of its high bimolecular rate constant, PTE is a good candidate for biosensor detection of nerve agents, topical skin protection, and decontamination of surfaces after exposure to OPs. The protective effect of PTE against OPs on cholinesterases and carboxylesterases was demonstrated [8]. PTE was structurally modified to improve its stereoselectivity and catalytic rate toward nerve agents [9].

X-ray crystallographic and metal chelation studies established the importance of the nature of the binuclear metal center[6, 9]. It was shown that the enzyme retains its catalytic activity when $Co^{2+}$, $Cd^{2+}$, $Mn^{2+}$ or $Ni^{2+}$ substituted $Zn^{2+}$ in native PTE. The rate of hydrolysis is dependent on the nature of the active site metals. For example, the $k_{cat}$ values for hydrolysis of paraoxon by recombinant PTE grown in $Zn^{2+}$, $Cd^{2+}$ and $Co^{2+}$ enriched medium are respectively 1520 $s^{-1}$, 2460 $s^{-1}$, and 4870 $s^{-1}$[6]. Substitution of naturally-occurring zinc ions by cobalt ions was reported to enhance the enzyme catalytic activity the most significantly [10], but is coupled to a decrease in stability [11].

It is noteworthy that some discrepancies exist in literature data, for ratio of kinetic parameters between $Co^{2+}$-containing and $Zn^{2+}$-containing PTE, ranging from 3 to 8 times [6, 10-14]. We investigate some possible cause of these puzzling differences. We carefully characterized the metal in the binuclear center of our preparation of recombinant enzyme using XRF and CCT-ICP-MS. We notably looked for the presence of $Fe^{2+}$ in the binuclear center, since it was reported that *Agrobacterium radiobacter* phosphotriesterase contains a $Fe^{2+}/Zn^{2+}$ binuclear center [15]. As the metals were well characterized, we focused on the stability of diluted PTE in kinetic assays and the effect of $Zn^{2+}$ and other divalent cations on the activity of PTE expressed either in $Zn^{2+}$-enriched medium (Zn-PTE) or in $Co^{2+}$-enriched medium (Co-PTE). Here we mark a difference between Co-PTE as defined above and $Co^{2+}$-containing PTE reconstituted from the apoenzyme. The goal of this study was to explore and understand some aspects of recombinant PTE and its mutant that are essential for optimal production and hydrolytic detoxification of pesticides and nerve agents.

## Material and methods

### *Expression and purification of PTE*

Wild type PTE was expressed in *E. coli* HMS 174 (DE3) pLysS (Novagen, Madison, WI, U.S.A.) carrying the plasmid pET17b-PTE*m*. pET17b was from Novagen as previously described [16]. The PTE*m* gene (kindly provided by D. Fournier, Université de Toulouse, France) was without the 29-aminoacid leader; it was shown to significantly improve the enzyme expression level [17]. The metal cation was introduced using a biosynthetic method. Bacterial cells were grown in a culture medium supplemented with the desired cation (final concentration 0.5 mM). Cations were added at the induction step to enhance the expression of active PTE. Subsequent steps were carried out at 4°C in 50 mM sodium borate pH 8.5, containing 0.1 mM of the appropriate salt ($ZnCl_2$ or $CoCl_2$). Wild-type PTE was purified according to the previously reported protocol [16], using an ion exchange chromatography on Fast Flow DEAE-Sepharose (Pharmacia Biotech, Uppsala, Sweden) and an affinity chromatography on Green 19-Agarose gel (Sigma). The enzyme was concentrated to 5 mg/mL using ultrafiltration units (Nanosep 10K Omega), and protein concentration was determined using the theoretical extinction coefficient calculated from the PTEm protein sequence using ProtParam ($\varepsilon_{280}$=1.29 $mg^{-1}.cm^{-1}$) (http://au.expasy.org/tools/protparam.html) and protein absorbance at 280 nm. Purity and homogeneity of PTE was checked by determining its specific activity and by SDS-PAGE. The molecular weight of PTE was determined by ESI-MS using formic acid as the dilution buffer. The oligomerization state of Zn- and Co-PTE was determined by gel filtration with an initial enzyme concentration of 1 mg/mL in 50 mM sodium borate buffer, pH 8.5 containing 100 mM KCl. 200 µL of sample was loaded on a Superdex 75 prep grade column with particules size of 34 µM with a fraction range from 3 to 70 kDa. Molecular weight standards were β-lactoglobulin (14.4 kDa), ovalbumin (43 kDa) and bovine serum albumin (67 kDa). Enzyme activity was measured for 5 µL of each fraction (250 µL) using 1 mM paraoxon as substrate.

### *Construction of PTE mutants*

H123A, H123I and H123N mutants of PTE were made by the PCR reverse method [18] using KOD Polymerase (Invitrogen). PCR fragments were purified with the QIAquick PCR purification kit (Qiagen) and cloned into the expression plasmid pET17b. The three mutants were expressed in *E. coli* BL21 (DE3) pLysS.

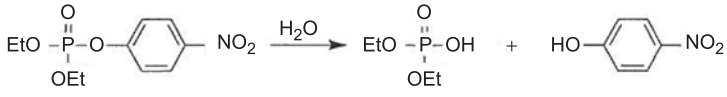


**Scheme 1.** Paraoxon hydrolysis.

***X-ray fluorescence measurements***

X-ray fluorescence was monitored with a solid-state RontecXFlash detector operating at the BM30A beam line. The detector was placed 90° from the incident X-ray beam to minimize scattering. The device server to run the detector on ESRF beam lines and the Graphical User Interface to monitor the X-ray fluorescence were developed by A. Beteva (ESRF) and J. Joly (BM30A), respectively. Fluorescence measurements were performed on both PTE (0.1 mM) expressed in the presence of $ZnCl_2$ and $CoCl_2$ in 50 mM sodium borate pH 8.5.

***Inductively coupled plasma mass spectrometry measurement***

Zinc, cobalt and iron were determined by CCT-ICP-MS Collision-reaction Cell Technology - Inductively Coupled plasma - Mass Spectrometry (Thermo, Dreieich, Germany). The instrument was operated using 1400 W RF power, 13 L/min as argon cool gas flow and 0.80 L/min for nebulizer and auxiliary argon gas flow. CCT cell gas was a mixture of helium and hydrogen (93-7% v/v) at a flow rate of 10 mL/min. Samples were diluted in nitric acid 1% (v/v) containing internal standards (Ga 50 µg/L and Rh 10 µg/L) before analysis. Standard nebulizer, Peltier cooled impact bead spray chamber and single piece quartz torch were used. Metal concentrations were determined using an external calibration curve containing Co (blank to 20 µg/L), Zn (blank to 500 µg/L) and Fe (blank to 200 µg/L). Measurements were performed for $Zn^{64}$ $Zn^{66}$, $Fe^{54}$, $Fe^{56}$ and $Co^{59}$ isotopes.

We determined the total concentration of $Co^{2+}$, $Zn^{2+}$, $Fe^{2+}$ in 50 mM sodium borate buffer, pH 8.5, containing 0.1 mM $CoCl_2$ with and without 0.11 mM PTE that was expressed in $CoCl_2$ enriched medium. The concentration of $Zn^{2+}$ and $Co^{2+}$ chelated by the enzyme was obtained by subtracting the values obtained in the presence of enzyme from the value given by the buffer (blank). In addition, we measured the total concentration of divalent cation in a solution containing PTE (0.06 mM) washed 5 times by ultrafiltration (2.5 × dilutions per cycle − Amicon PM10) with 50 mM sodium borate buffer, pH 8.5. The washing buffer recovered from the last cycle was used as the blank.

***Stability of Zn-PTE and Co-PTE under assay conditions***

The enzyme activity of 0.2 nM PTE with paraoxon (3.5 mM; Sigma-Aldrich) as the substrate was followed by monitoring the release of *p*-nitrophenol at 400 nm ($\varepsilon = 17{,}000$ $M^{-1}cm^{-1}$) in 15% methanol, 50 mM sodium borate buffer, pH 8.5 at 30°C, using a Tecan Safire microplate spectrophotometer. The rate of hydrolysis remained linear during the test (10 min monitoring). We tested the activity of both PTE, 2 min after they were diluted in assay buffer with or without additives, 0.1% β-lactoglobulin and 50µM $ZnCl_2$.

***Determination of Kinetic and inhibition constants in the presence of divalent cations***

All kinetics measurements were performed using a Tecan Safire microplate spectrophotometer at 30°C. Hydrolysis of paraoxon up to 3.5 mM by 0.2 nM PTE was performed in 15% methanol, 50 mM sodium borate at pH 8.5 with 0.1% of β-lactoglobulin for stabilization purpose and in the presence of 0 to 0.5 mM $ZnCl_2$, 0 to 3 mM $NiCl_2$ or 0 to 2 mM $CoCl_2$/$CdCl_2$/Mg/$Cl_2$/$FeSO_4$. Inhibitions were characterized by Lineweaver-Burk and Dixon plots. The analysis of $ZnCl_2$ inhibition was treated as a special case because at pH 8.5, $ZnCl_2$ forms colloid particles that interact with the enzyme. This leads to partial non-competitive inhibition. Considering the equilibrium between the enzyme (E) and n colloid particles (I):

$$E + n.I \quad EI_n$$

We assume that the binding of each particle is equivalent:

$$Ki = \frac{[E]\cdot[I]}{[EI]} = \frac{[EI]\cdot[I]}{[EI_2]} = \frac{[EI_{n-1}]\cdot[I]}{[EI_n]}$$

We can define: $$Ki^n = \frac{[E]\cdot[I]^n}{[EI_n]}$$

Then, the non-competitive partial inhibition by n particles can be described as follow:

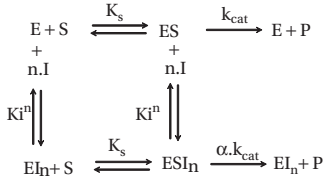


As the concentration of $Zn(OH)_2$ colloid [I] is equal to $\gamma[ZnCl_2]$, we define $Ki_{app}$ the apparent inhibition constant of $ZnCl_2$ as $Ki = \gamma Ki_{app}$. Further assuming that $K_s = K_m$ we derive the following equation:

$$\frac{v}{E_t} = \frac{k_{cat}[S]}{[S]+K_m}\cdot\frac{Ki_{app}^n + \alpha\cdot[ZnCl_2]^n}{Ki_{app}^n + [ZnCl_2]^n} \qquad (1)$$

[S] is the substrate concentration, n the number of equivalent of colloidal particles, v the initial velocity, $k_{cat}$ the turnover number, $E_t$ the enzyme concentration, $K_m$ the Michaelis constant, $Ki_{app}$ the apparent inhibition constants of $ZnCl_2$ and α the partiality coefficient. $E_t$ was determined by UV absorbance assuming that 100% of enzyme molecules were active. The kinetic parameters were determined by simultaneously fitting $v/E_t$ for different [$ZnCl_2$] and [S] according to Equation (1) using GOSA-fit, a fitting software based on simulated annealing algorithm (BioLog, Toulouse, France; http://www.bio-log.biz).

***Fluorescence Measurement and data analysis***

The fluorogenic analogue of VX, O,O-(3-chloro-4methyl-2oxo-2h-chromen-7-yl) ethylmethylphosphonate[19], was

a gift from Dr William R. Gareth (Synthetic Chemistry Team, DSTL Porton Down, U.K). The hydrolysis of the VX analogue by PTE was followed by the change in fluorescence at 460 nm, with a wavelength excitation at 350 nm using a SFM25 Kontron Instruments at 25°C. The hydrolysis of 6 μM VX analogue was performed in 15% isopropanol, 50 mM sodium borate at pH 8.5, containing 0.1% of β-lactoglobulin with 3.5 nM Co-PTE, at different concentrations of $ZnCl_2$ (0, 0.02, 0.08, 0.25, 0.5, 0.75, 1, 1.5, 2 mM). The initial velocity was measured by following the release of 3-chloro-7-hydroxy-4--methylcoumarin during 100 s. The $IC_{50}$ values for $Zn(OH)_2$ colloid inhibition of Co-PTE activity was determined by fitting the data to the Equation (2) where $v_i$ is the reaction velocity at different zinc concentrations [I], $v_0$ is the initial velocity in the absence of inhibitor, $IC_{50}$ is the analytical concentration in $ZnCl_2$ required to achieve 50% inhibition and a is a partiality factor. At pH 8.5, most of $Zn^{2+}$ forms $Zn(OH)_2$.

$$\frac{v_i}{v_o} = \frac{1-a}{1+\frac{[I]}{IC_{30}}} + a \qquad (2)$$

## Results and discussion

### *Oligomerization state*

The molecular weight of PTE monomer determined by ESI-MS under acidic conditions is 36,286 ± 5 Da. This value is in agreement with the molecular weight from the amino acid sequence (36,292 Da). Gel filtration chromatography of Zn- and Co-PTE at concentration of 1 mg/mL indicates a value about 36 ± 4 kDa for the active enzyme (Figure 1). Gel filtration was performed at different ionic strength (0 to 200 mM KCl) and in presence of various concentrations of $Zn^{2+}$ and $Co^{2+}$ (up to 2 mM) without changes in chromatogram profiles. All the enzyme activity was located in the single peak (not shown). Thus, active Zn- and Co-PTE are clearly monomeric under the kinetic assay conditions. The oligomerization state does not seem to be dependent on the nature of the divalent cation. This is in agreement with reported results on gel filtration of Zn-PTE expressed using the Baculovirus system [20], Zn-PTE homology protein from *E. coli* [21] and PTE from *Flavobacterium* [22]. However, it is generally assumed, that Zn-PTE is dimeric in solution because it crystallizes as a dimer. This claim were apparently supported by ultracentrifugation [5] and gel filtration experiments [23], though data and experimental details were not shown.

### *Binuclear center characterization*

It is important to systematically and fully characterize the binuclear center to rationalize the kinetics of recombinant PTE because the activity is dependent on the nature of divalent metal and the level of metal substitution change from one preparation of enzyme to the other. The determination of the nature of cations in our preparations of Zn-PTE and

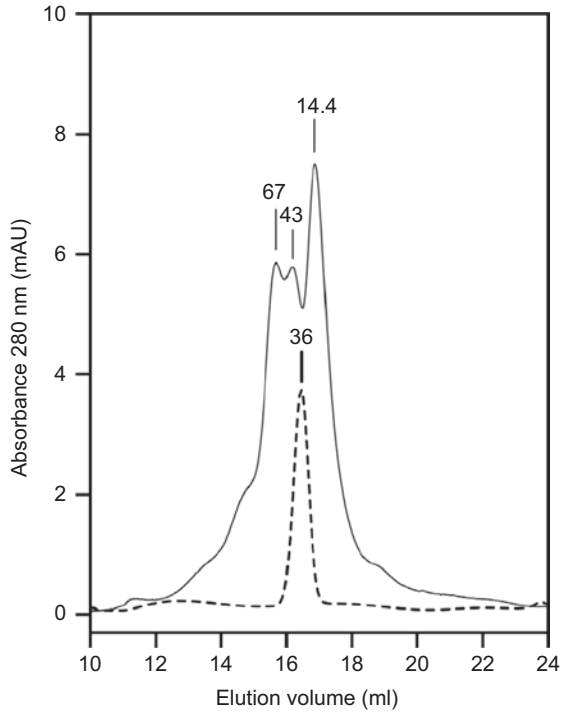


**Figure 1.** Typical gel filtration of Co-PTE and Zn-PTE. The size of Zn- or Co-PTE in solution was determined by gel filtration with an initial enzyme concentration of 1 mg/mL and a volume sample of 200 μL. A gel filtration of Co-PTE is shown. The absorbance profiles of Co-PTE (bold dashed line) and molecular weight standards (thin line) were recorded at 280 nm. The molecular weight of β-lactoglobulin (14.4 kDa), ovalbumin (43 kDa) and bovine serum albumin (67 kDa), and the estimated value of Co-PTE (36 kDa) are indicated at the top of each corresponding peaks.

Co-PTE was performed using X-ray fluorescence (Figure 2). The spectrum of Zn-PTE shows a major peak at 8600 eV with a fluorescence intensity of 790 counts, and a slight peak of 120 counts at 9530 eV. These peaks correspond to X-ray fluorescence of ZnKα and ZnKβ respectively. A small peak at 6400 eV with a fluorescence intensity of 60 counts may correspond to FeKα, suggesting trace of $Fe^{2+}$ in the enzyme preparation. No other fluorescence peaks for divalent cations were observed, confirming that PTE expressed in medium supplemented with $ZnCl_2$ contains two zinc cations in the active site. This result is in agreement with high-resolution X-ray structure data [24]. The Zn peak is still present in the Co-PTE spectrum with a fluorescence intensity of 245 counts for ZnKα peak and 40 counts for ZnKβ peak. Another peak was observed at 6930 eV with a fluorescence intensity of 130 counts, corresponding to the emission of CoKα. We also observed a weak signal for CoKβ. The faint peak at 6400 eV, assumed to correspond to FeKα, is still present. Therefore, our sample of PTE expressed in medium supplemented with $CoCl_2$ contains both cobalt and zinc cations. This is in agreement with FAAS analysis found in the literature [13]. It differs from $Co^{2+}$-containing PTE prepared from the apoenzyme, which contains two $Co^{2+}$ according to analysis based on atomic absorption spectrophotometry [6]. Surprisingly, it was reported that the crystal structure of the H254R mutant of PTE expressed

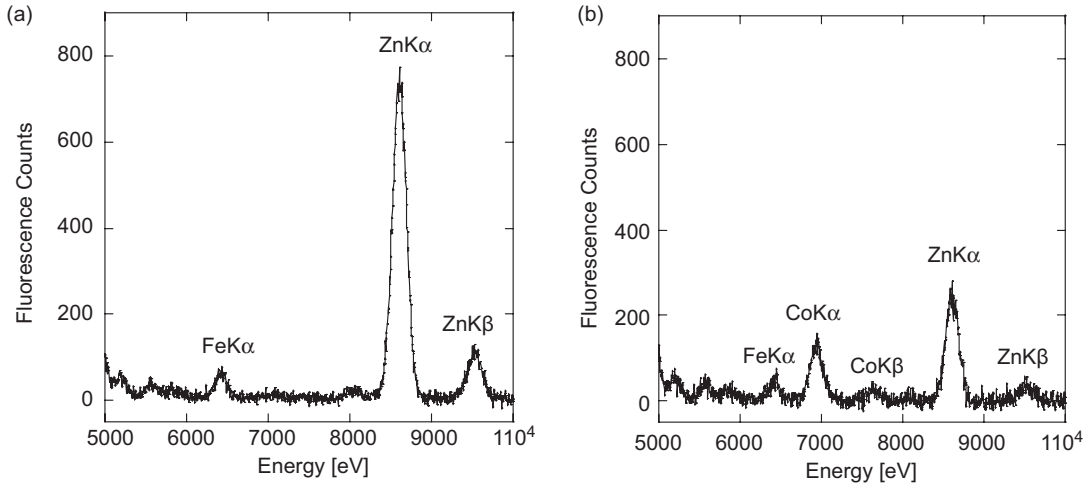


**Figure 2.** X-Ray Fluorescence spectrum of recombinant Zn-PTE and Co-PTE. XRF spectrum for energy between 5 and 10 KeV of 0.1 mM Zn-PTE (a) and 0.1 mM Co-PTE (b).

in $Co^{2+}$-enriched medium contains two $Co^{2+}$ [14]. However no metal analysis was performed and as it is not possible to discriminate between $Zn^{2+}$ and $Co^{2+}$ from the electronic density, we doubt that the binuclear center in this crystal structure is homogenous.

CCT-ICP-MS analysis was performed in order to accurately quantify the relative amount of divalent cations in the binuclear active site center of Co-PTE. The concentrations of $Zn^{2+}$ and $Co^{2+}$ were respectively 110 μM and 100 μM in a sample containing 110 μM Co-PTE. Co-PTE contained one equivalent of $Zn^{2+}$ and one equivalent of $Co^{2+}$. The recombinant enzyme does not contain significant amount of $Fe^{2+}$ (<2 μM), but it does not rule out that the native enzyme from *Pseudomonas* contains $Fe^{2+}$. In addition, Enzyme washed using ultra-filtration and diluted at 50 μM contained 1 equivalent of $Zn^{2+}$ (50 μM) but 0.7 equivalent of $Co^{2+}$ (35 μM). This result indicates that $Co^{2+}$ readily dissociates upon dilution and suggests that $Co^{2+}$ likely binds at the more solvent exposed and labile β-metal site while $Zn^{2+}$ is located at the more buried α-metal site. This is reminiscent to Cd-PTE from *Pseudomonas* sp. WBC-3, which also contains a mixed hybrid binuclear zinc center, in which the zinc ions at the β-metal site is replaced by cadmium [25].

Altogether, these results and literature data show that bacterial expression of PTE in $CoCl_2$-enriched medium yields a heterogenous binuclear center, even if $CoCl_2$ is added during the purification steps. Homogenous $Co^{2+}$-containing PTE is more reproducibly obtained by reconstitution from the apoenzyme, but the enzyme displays a tendency to loose the cation at the β-metal site upon dilution, yielding partially metallated unstable populations of enzyme.

### *Stability of Zn-PTE and Co-PTE under the conditions of kinetic measurements*

The catalytic constants of Zn-PTE and Co-PTE vary significantly within reports. For example, the $k_{cat}$ values for reconstituted Zn-PTE were found to be 780 $s^{-1}$ [26] and 2430 $s^{-1}$ [6]. In addition to heterogeneity of the binuclear center for enzymes expressed in metal enriched medium, a possible cause for such a large variation may simply be related to the lack of information regarding the protein titration method used. Knowledge of active site concentration is critical to determine real kcat. Indeed, in recent literature, citations in cascade are used to describe the titration method. These citations finally lead to the earliest work on expression of PTE in baculovirus but not in *E. coli* [20]. In this work, absorbance at 280 nm (without reported $\varepsilon_{280nm}$) and bicinchoninic assay were cited as the methods used for crude samples, but no details were given for the purified enzyme.

Another possible cause of these fluctuations could be that additives have not been systematically used to stabilize PTE upon dilution required for kinetic measurements. We tested the influence of putative stabilizers of PTE, $Zn^{2+}$ the enzyme cofactor, and β-lactoglobulin that provides a protein environment. The maximum activity was obtained in the presence of 0.1% (w/v) β-lactoglobulin (Figure 3). We verified, by pre-coating tubes with β-lactoglobulin, that loss of activity was not due to adsorption of the enzyme on tube walls. Because the loss activity apparently occurs during the dilutions and before substrate is added, the rate of hydrolysis remains linear during the time of the activity test (10 minutes). This indicates that paraoxon stabilizes PTE, which is quite a usual effect for substrates. Without additives, both PTEs dramatically loose about 90% of their activity upon dilution. 50 μM $ZnCl_2$ has a modest stabilizing effect, as Zn-PTE and Co-PTE retain respectively 38% and 27% of their activity 2 minutes after dilution. However, there are neither additives nor synergistic effect of $ZnCl_2$ and β-lactoglobulin. Otherwise, adding $ZnCl_2$ to the enzyme stabilized by β-lactoglobulin results in 10% and 20% decrease in activity for Co-PTE and Zn-PTE, respectively. Noteworthy, $ZnCl_2$ has an inhibitory effect when a protein environment stabilizes PTE. This inhibition is characterized later in this paper.

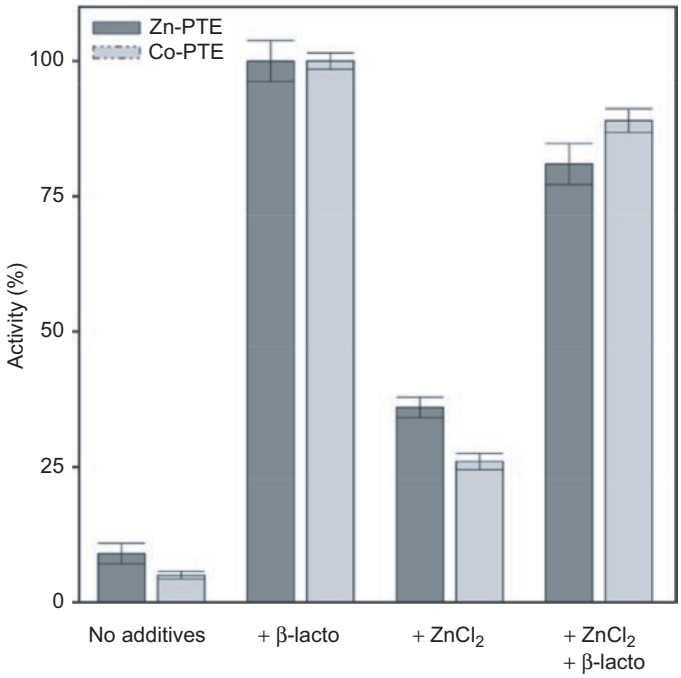


**Figure 3.** Stability of Zn-PTE and Co-PTE under assay conditions. Paraoxon hydrolysis of Zn-PTE and Co-PTE in the absence of additives, with 0.1% of β-lactoglobulin, with 50 μM $ZnCl_2$ and with both additives, 5 minutes after dilution of the stock enzyme.

It was shown that during the time course of bacterial expression, newly synthesized PTE is unstable until the binuclear center is formed [27]. Here, we observed that the presence of $Zn^{2+}$ in solution slows down the inactivation that occurs at low enzyme concentration and in the absence of β-lactoglobulin. We assume that at low concentration, there is a shift toward population of conformers that tend to loose their metal cations, leading to unstability, complete unfolding and aggregation. In this case, the presence of $Zn^{2+}$ would help to maintain highly populated metal sites, slowing down the inactivation process. Remarkably, the presence of a sufficient protein environment, like that provided by 0.1% β-lactoglobulin, stabilizes PTE probably by preventing the shift toward unstable conformers. It follows that 0.1% β-lactoglobulin has to be systematically added in medium for enzyme dilutions and kinetic assays.

***Paraoxon hydrolysis by stabilized Zn-PTE and Co-PTE***

Adding 0.1 % β-lactoglobulin to dilutions of PTE for assays allowed to obtained reproducible kinetic results. PTE-catalyzed hydrolysis of paraoxon obeys the Michaelis-Menten model (Figure 4). The rate of paraoxon hydrolysis catalyzed by Co-PTE was 3 times faster ($k_{cat}$ = 4010 ± 40 $s^{-1}$) than the one catalyzed by Zn-PTE ($k_{cat}$ = 1290 ± 10 $s^{-1}$) at pH 8.5 and 30°C. These values are in agreement with some reported data [6], although pH and temperature conditions were different and the protein titration method was probably different. Catalytic parameters, listed in Table 1, show that the efficiency ($k_{cat}/K_M$) of Co-PTE toward paraoxon is 2-fold higher than that of Zn-PTE. This shows

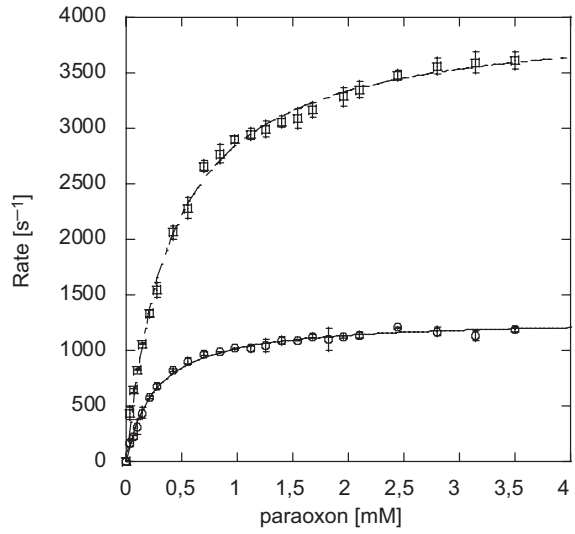


**Figure 4.** Michaelis-Menten Plot of paraoxon hydrolysis by Zn-PTE and Co-PTE. Initial reaction rate plotted against substrate concentration for paraoxon hydrolysis by PTE purified with $Zn^{2+}$(○) and $Co^{2+}$(□).

that a single $Co^{2+}$ in the active site already provides a significant enhancement of the catalytic efficiency compared to Zn-PTE.

***Effect of metal cations excess on PTE activity***

We observed that $ZnCl_2$ has an inhibitory effect on PTE in the sub-millimolar range. This was previously noted [6]. As divalent cations are cofactors that are added in excess to buffers during expression, purification, kinetic assays, and in decontamination solutions, we wanted to clarify their possible inhibitory effect on the enzyme activity. The paraoxon hydrolysis activity of both Co-PTE and Zn-PTE was measured in the presence of increasing concentrations of $Zn^{2+}$, $Co^{2+}$, $Cd^{2+}$, $Mg^{2+}$, $Ni^{2+}$ chloride and $Fe^{2+}$sulfate. The activity of both PTEs remained unchanged upon addition of $CoCl_2$, $CdCl_2$, $FeSO_4$ and $MgCl_2$ up to 2mM. However, $ZnCl_2$ inhibited the hydrolysis activity of both Zn-PTE and Co-PTE (Figure 5). We wondered whether inhibition arises from interactions of additional zinc ions with the binuclear center or with another site and decided to investigate this side effect of zinc excess. We first verified that this inhibition was not dependent on the ionic strength or to oligomerization. High ionic strength did not alter the inhibitory effect of $ZnCl_2$ in borate buffer containing up to 300 mM NaCl. The effect of $ZnCl_2$ could not be due to a change in the oligomerization state or aggregation of PTE because no peak shift or new peak was observed at concentrations up to 2 mM $ZnCl_2$. Actually, we figured out that at pH 8.5, the inhibition is likely not related to free $Zn^{2+}$ ions present in the solution. At this pH, the solubility product constant of $Zn^{2+}/Zn(OH)_2$ is $8x10^{-17}$ (CRC Handbook of Chemistry and Physics 80th Ed; at 30°C), so that the concentration of $Zn^{2+}$ in solution is less than 8 μM, and $[Zn(OH)_2] \approx [ZnCl_2]$ in the concentration range of the inhibition. Besides, cloudy precipitate of $Zn(OH)_2$ was clearly visible when concentrations of $ZnCl_2$ higher than 1 mM were used in assays. Therefore, it is more

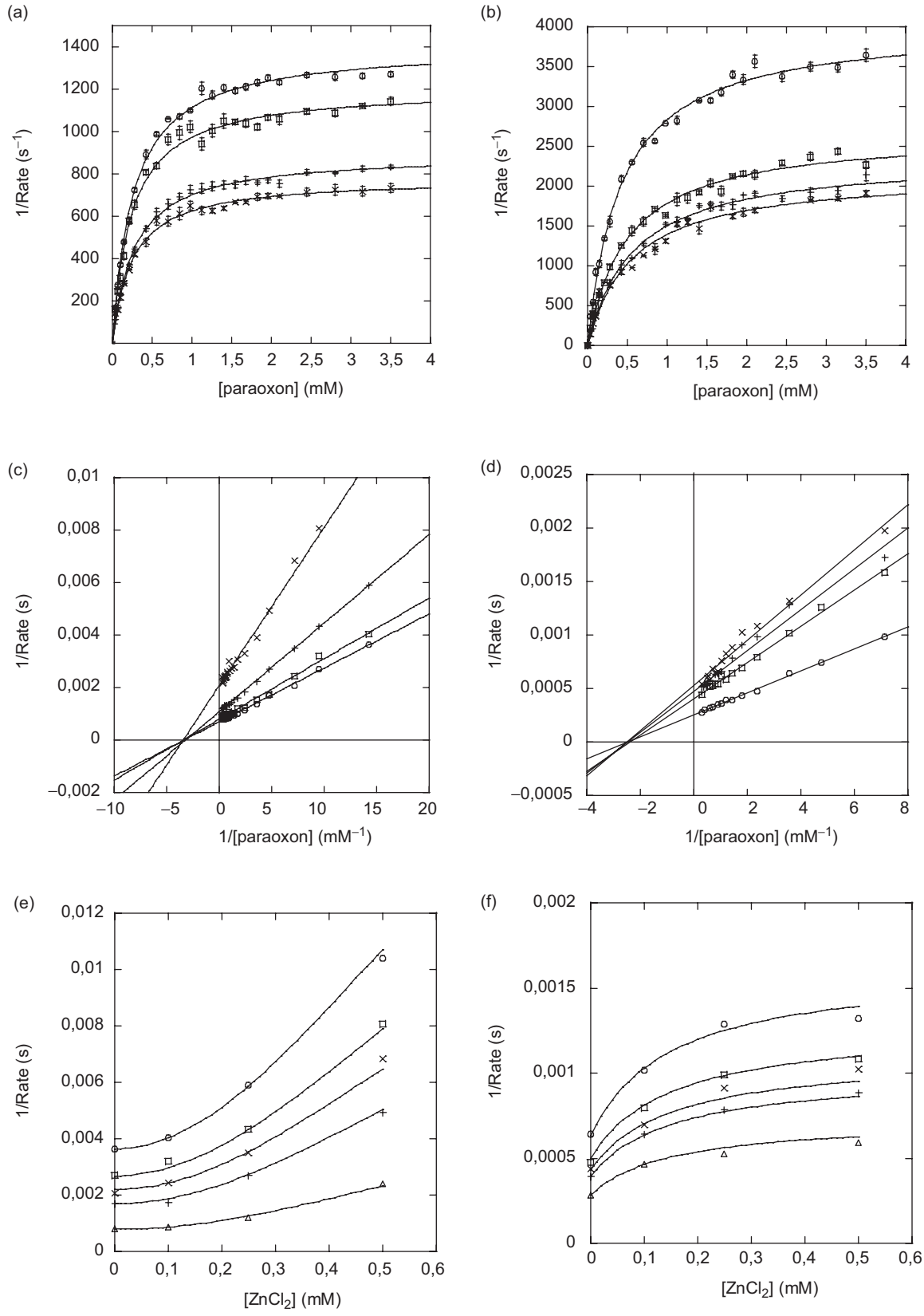


**Figure 5.** Inhibition of paraoxon hydrolysis of Co-PTE and Zn-PTE by $ZnCl_2$. Reaction rate versus paraoxon concentration for Zn-PTE (a) and Co-PTE (b) in the absence (○) and presence of 0.1 mM (□), 0.25 mM (×) and 0.5 mM (+) $ZnCl_2$. Lineweaver-Burk plot of Zn-PTE (c) and Co-PTE (d) activities in the absence (○) and presence of 0.1 mM (□), 0.25 mM (×) and 0.5 mM (+) $ZnCl_2$. Dixon plots of Zn-PTE (e) and Co-PTE (f) with0.28 mM (○), 0.42 mM (□), 0.56 mM (×), 0.7mM (+), 3.5 mM (△) paraoxon. The best-fit curves or lines were determined using GOSA-fit and Equation (2), with n=2 for Zn-PTE and n=1 for Co-PTE.

**Table 1.** Paraoxon hydrolysis catalyzed by recombinant wild type PTE expressed in the presence of zinc and cobalt chloride and mutants expressed in the presence of cobalt chloride.

| | $k_{cat}$ ($s^{-1}$)* | $K_m$ (mM) | $k_{cat}/K_m$ ($M^{-1}s^{-1}$) | $Ki_{app}$ (μM) | n | Partial factor (*a*) |
|---|---|---|---|---|---|---|
| Zn-PTE | 1290±10 | 0.26±0.01 | $5\times10^6$ | 155±10 | 2 | 0.50±0.01 |
| Co-PTE | 4010±40 | 0.40±0.02 | $10\times10^6$ | 52±6 | 1 | 0.45±0.02 |
| Co-His123Asn | 1610±30 | 0.34±0.03 | $4.7\times10^6$ | 230±50 | 1 | 0.30±0.05 |
| Co-His123Ala | 390±5 | 0.39±0.03 | $1\times10^6$ | 300±100 | 1 | 0.47±0.07 |
| Co-His123Ile | 50±1 | 0.36±0.03 | $0.14\times10^6$ | 630±50 | 1 | 0 |

* Determined from $V_{max} = k_{cat}[E_t]$, assuming that 100% of enzyme molecules are active; these values are therefore the minimal values of $k_{cat}$.



likely that inhibition was due to $Zn(OH)_2$ colloidal particles whose effective concentration is $\gamma[ZnCl_2]$, $\gamma$ being an activity coefficient. It follows that inhibition constants for this type of inhibition must be regarded as apparent phenomenologic parameters.

Since the solubility product constant of $Ni^{2+}/Ni(OH)_2$ is $1.5\times10^{-15}$ (CRC Handbook of Chemistry and Physics 80th Ed; at 30°C), corresponding to a maximum concentration of 150 μM at pH 8.5, a similar effect occurs during inhibition experiment using $NiCl_2$. Lineweaver-Burk plots show that colloidal $Ni(OH)_2$ is a non-competitive inhibitor of Co-PTE with apparent Ki = 3.0 ± 0.2 mM, n=1 and α=0 (plot not shown).

Lineweaver-Burk plots show that colloidal $Zn(OH)_2$ is a non-competitive inhibitor of Zn-PTE and Co-PTE (Figure 5c and 5d), $K_m$ remains unaffected whereas $k_{cat}$ decreases. In addition, the curvature of the Dixon plots reveals that inhibition of Zn-PTE and Co-PTE are non linear (Figure 5e and 5f). The hyperbolic and parabolic shapes of the Dixon plots for Co-PTE and Zn-PTE, respectively, can be interpreted as a partial inhibition and multiple binding of colloidal particles mixed with partial inhibition, respectively.

We determined that two equivalents of $Zn(OH)_2$ colloidal particles (n=2) are involved in inhibition of Zn-PTE, $Ki_{app}$ = 155±10 μM with a partiality coefficient of 0.50±0.01 and a single equivalent for Co-PTE (n=1), $Ki_{app}$ = 52±6 μM with a partiality coefficient of 0.45±0.02 (Table 1). The fit of non-linear Dixon plots, using the parameters determined above (curved line; Figure 5e and 5f), shows the accuracy of the prediction.

We further investigated the inhibition of PTE by zinc with a structurally different substrate in order to definitively exclude the possibility that inhibition results from interaction of $Zn(OH)_2$ colloid with paraoxon, causing substrate depletion. We used a fluorogenic substrate, O,O-(3-chloro-4methyl-2oxo-2H-chromen-7-yl)ethylmethylphosphonate, that is a mimic of the nerve agent VX [19]. The VX-analogue hydrolysis activity of Zn-PTE was too slow to determine an accurate median inhibitory concentration ($IC_{50}$), but it was sufficient for Co-PTE. Increasing concentrations of $ZnCl_2$ inhibit Co-PTE with an $IC_{50}$=0.53 ± 0.08 mM and a partiality coefficient a = 0.68 (Figure 6). Based on the above results about inhibition of paraoxon hydrolysis, we can reasonably assume that inhibition of hydrolysis of the VX analogue is non competitive, so that $IC_{50}$=Ki, one order of magnitude higher than for paraoxon. Thus, $Zn(OH)_2$ colloid inhibition

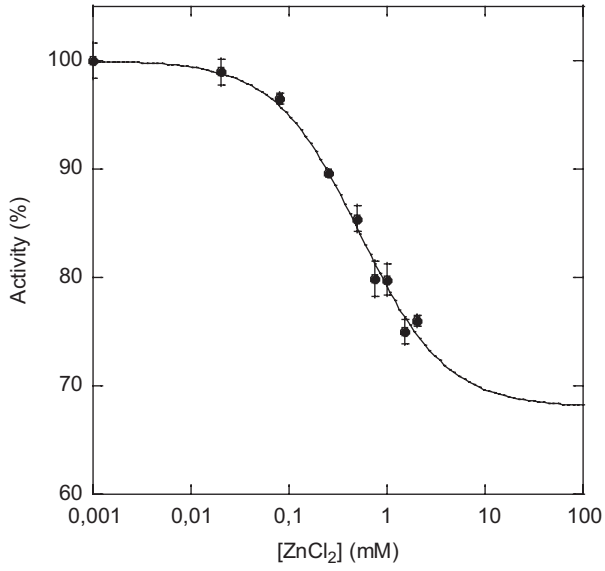


**Figure 6.** Inhibition of Co-PTE-catalyzed hydrolysis of an analogue of VX by $ZnCl_2$2. Hydrolysis of an analogue of VX by Co-PTE in the presence of increasing concentrations of $ZnCl_2$ up to 2 mM.

is not limited to inhibition of paraoxon hydrolysis, but its strength is dependent on the nature of the substrate.

The non-competitivity and partiality of inhibition suggests an allosteric effect due to binding of $Zn(OH)_2$ particles on the surface of PTE. Since $Zn(OH)_2$ forms a colloid suspension in solution, it is rather difficult to rationalize its inhibitor properties at the molecular level, especially the fact that two equivalents are necessary to inhibit Zn-PTE while one equivalent is sufficient for Co-PTE. However, allosteric effects are related to shift in equilibrium between conformers [28] as recently confirmed by experimental and theoretical studies [29]. Thus, we may assume that multiple binding of $Zn(OH)_2$ particles alters the dynamic equilibrium of PTE by interfacial interactions.

### *Effect of His123 mutations on the stability of Co-PTE and zinc hydroxide interactions.*

At some point, we thought that the species involved in the noncompetitive inhibition was $Zn^{2+}$. Therefore, we looked for a putative binding site for $Zn^{2+}$. Coordination of $Zn^{2+}$ systematically involves in order of occurrence, Histidine, Cysteine and Aspartate/Glutamate and a careful analysis of the crystal structure of PTE shows that there is a single

histidine residue located at the surface (His123), with two carboxylic residues nearby (Asp121 and Glu48) (Figure 7). We were assuming that all, or a couple of these residues may participate to the coordination sphere of $Zn^{2+}$. Actually, mutant His123Asn was already studied in earlier work in attempt to identify residues involved in $Zn^{2+}$ catalytic binding site. At that time, a 30% decrease in kcat was reported for reconstituted Co-PTE without change of $K_M$ [30]. No change in $K_M$ suggests that mutations of this surface residue affect the conformational equilibrium of the enzyme, with a conformation of enzyme that is fully active and at least another conformation that is less active. Although His123 is at the opposite side of the catalytic site, it is only 12 Å away from a recently identified allosteric site [14], thus supporting again the hypothesis that His123 may affect the allosteric machinery. In addition, other mutations distant from the active site have been shown to affect catalytic properties [31], showing that the catalytic activity is dependent on PTE's conformational dynamics.

Despite the nature of the inhibition by $Zn(OH)_2$ did not justify looking for a true $Zn^{2+}$ binding site, we mutated His123 into asparagine, alanine and isoleucine and checked if $Zn(OH)_2$. Mutations into asparagine and isoleucine were chosen because the former is the least disruptive residue as it is the closest isoster of histidine, and the latter was expected to favorably interact with Ile44 and Thr39 side chains preventing disruption of the structure.

Purification yields of the mutants expressed in $CoCl_2$-enriched medium were much lower than those of the wild type enzyme (about 200 times less), supporting the contention that the mutations strongly affect the overall conformational stability of the enzyme. The impact of the mutations on Co-PTE activity toward paraoxon is summarized in Table 1. While $K_M$ remains remarkably unaffected, the catalytic constant $k_{cat}$ decreased 2.5- 10- and 80-fold for mutants His123Asn, His123Ala and His123Ile, respectively. Such a change in kcat without affecting $K_M$ strongly suggests that the mutant enzyme exists under at least two conformational forms, one that can bind paraoxon like the wild type enzyme and is fully active and one that cannot bind and hydrolyze paraoxon. Thus, the mutation induces a shift toward population of conformers that are less efficient at hydrolyzing paraoxon.

$Zn(OH)_2$ inhibition was significantly altered by the mutations, the apparent Ki being about one order of magnitude higher than that for wild type Co-PTE (Table 1). Such an increase in Ki indicates that $Zn(OH)_2$ colloidal particles bind to a specific conformation that was affected by the

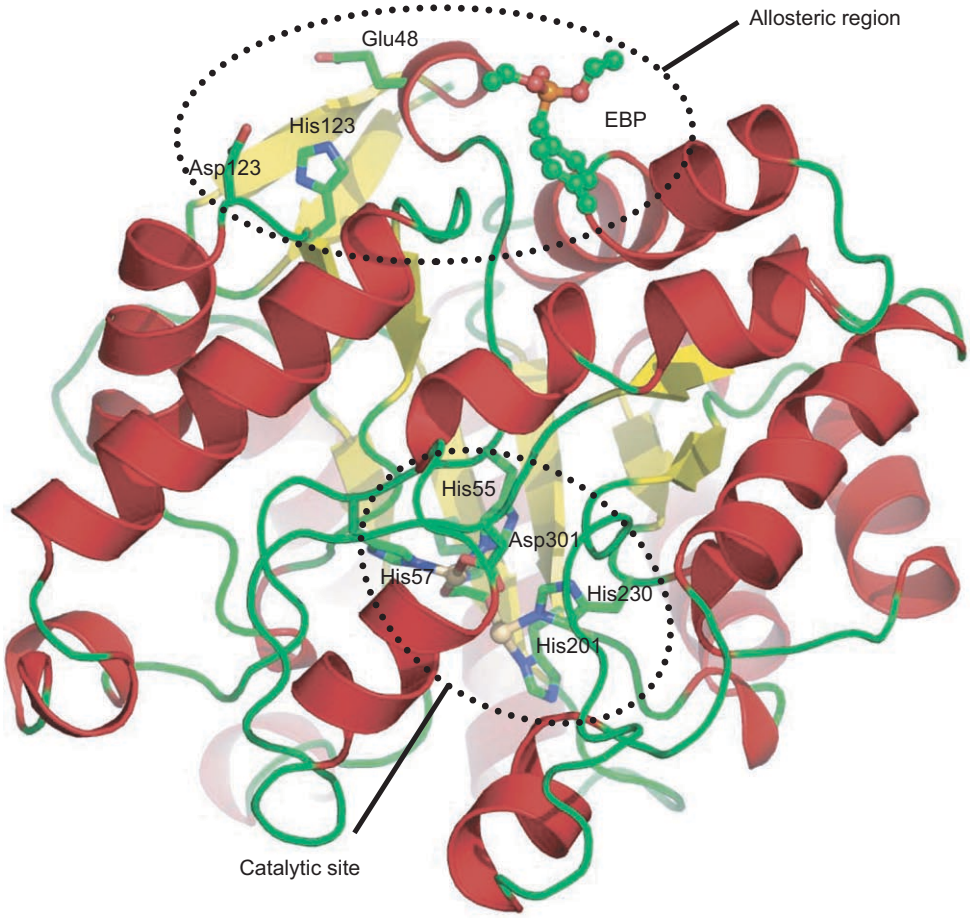


**Figure 7.** Crystal structure of PTE. Cartoon view of the crystal structure of PTE-Cd/Cd (pdb code 1PSC). α-Helixes are in red and β-sheets in yellow. The allosteric ligand EBP is represented in ball and stick. Residues from the putative Zn binding site and the catalytic site are in stick.

mutation. Besides, His123Ile mutant lost the partiality of inhibition which means that for this particular mutant, colloidal $Zn(OH)_2$ binds to a non productive conformer of the enzyme mutant.

Altogether, we have three independent observations - lower expression yield - decrease in kcat value without change in $K_M$ - decrease in sensitivity to inhibition by $Zn(OH)_2$, indicating that the mutation of His123 alter the dynamic equilibrium between active and unstable inactive conformations.

## Conclusions

We showed that recombinant Co-PTE is unambiguously monomeric under the conditions of kinetic assay while dimerization may occur at higher concentrations encountered for making crystals or in ultracentrifugation experiments.

In order to fully characterize our recombinant enzyme preparations before performing kinetic assays, we determined the composition of the binuclear center of Zn-PTE and Co-PTE, qualitatively by X-ray fluorescence and quantitatively by CCT-ICP-MS and found 2 equivalents of $Zn^{2+}$, no $Fe^{2+}$ for recombinant Zn-PTE, while Co-PTE contains one equivalent $Zn^{2+}$ and one equivalent $Co^{2+}$, the later being located most likely in the labile β-site. Recombinant Co-PTE is two times more efficient than recombinant Zn-PTE despite containing a single $Co^{2+}$ cation. Better efficiency is expected for Co-PTE containing two $Co^{2+}$ obtained by reconstitution from the apoenzyme, but instability of the apoenzyme might pose problems for large scale production of Co-PTE for decontamination purposes.

Both recombinant enzymes are unstable upon dilution and enzymatic assay, and require a stabilizing protein environment that was only used in two recent works [31, 32]. In addition, formulations of the wild type enzyme for decontamination purpose should also provide a stabilizing environment to maintain optimal activity and storage stability.

We characterized a non competitive partial inhibition of $ZnCl_2$, related to interactions with $Zn(OH)_2$ colloidal particles at the pH commonly used in kinetic assays. This inhibition was overlooked in previous studies. To achieve maximal activity, it is important to avoid addition of $ZnCl_2$ in medium during kinetic assays.

Mutation effects of solvent-exposed His123 suggest that the population of conformers of this mutant is shifted away from the productive and stable population compared to that of the wild type. Effort should be pursued to find mutations with the opposite effect, i. e., causing a shift toward the productive population, in the line of the work already engaged by certain groups [27, 31].

To date, practical applications have been limited mostly by the poor reproducibility of scaled production of recombinant PTE, related to the problems of expressing stable and fully metallated enzyme. This paper addresses some aspects of these issues that have slowed down the development of PTE into an efficient enzyme decontamination agent.

## Acknowledgements

The authors thanks Dr. W.R. Garreth (Synthetic Chemistry Team, DSTL Porton Down, U.K) for the gift of O,O-(3-chloro-4methyl-2oxo-2h-chromen-7-yl) ethylmethylphosphonate.

***Declaration of interest*:** This work was supported by DGA grant 03co10-05/PEA 010807 to PM and DGA grant 08co501 to FN. DR is under contract with the German Bundesministerium der Verteidigung (M/SAB 1/7 A004).

## References

1. Dumas DP, Durst HD, Landis WG, Raushel FM, Wild JR. Inactivation of organophosphorus nerve agents by the phosphotriesterase from Pseudomonas diminuta. *Arch Biochem Biophys* 1990;277:155–9.
2. Raushel FM.Bacterial detoxification of organophosphate nerve agents. *Curr Opin Microbiol* 2002;5:288–95.
3. Ghanem E, Raushel FM.Detoxification of organophosphate nerve agents by bacterial phosphotriesterase. *Toxicol Appl Pharmacol* 2005;207:459–70.
4. Afriat L, Roodveldt C, Manco G, Tawfik DS.The latent promiscuity of newly identified microbial lactonases is linked to a recently diverged phosphotriesterase. *Biochemistry* 2006;45:13677–86.
5. Benning MM, Kuo JM, Raushel FM, Holden HM.Three-dimensional structure of phosphotriesterase: an enzyme capable of detoxifying organophosphate nerve agents. *Biochemistry* 1994;33:15001–7.
6. Omburo GA, Kuo JM, Mullins LS, Raushel FM.Characterization of the zinc binding site of bacterial phosphotriesterase. *J Biol Chem* 1992;267:13278–83.
7. Jackson CJ, Foo JL, Kim HK, Carr PD, Liu JW, Salem G, Ollis DL.In crystallo capture of a Michaelis complex and product-binding modes of a bacterial phosphotriesterase. *J Mol Biol* 2008;375:1189–96.
8. Tuovinen K, Kaliste-Korhonen E, Raushel FM, Hanninen O.Protection of organophosphate-inactivated esterases with phosphotriesterase. *Fundam Appl Toxicol* 1996;31:210–7.
9. Chen-Goodspeed M, Sogorb MA, Wu F, Raushel FM.Enhancement, relaxation, and reversal of the stereoselectivity for phosphotriesterase by rational evolution of active site residues. *Biochemistry* 2001;40:1332–9.
10. Hong SB, Raushel FM.Metal-substrate interactions facilitate the catalytic activity of the bacterial phosphotriesterase. *Biochemistry* 1996;35:10904–12.
11. Rochu D, Viguie N, Renault F, Crouzier D, Froment MT, Masson P.Contribution of the active-site metal cation to the catalytic activity and to the conformational stability of phosphotriesterase: temperature- and pH-dependence. *Biochem J* 2004;380:627–33.
12. Shim H, Raushel FM.Self-assembly of the binuclear metal center of phosphotriesterase. *Biochemistry* 2000;39:7357–64.
13. Di Sioudi B, Grimsley JK, Lai K, Wild JR.Modification of near active site residues in organophosphorus hydrolase reduces metal stoichiometry and alters substrate specificity. *Biochemistry* 1999;38:2866–72.
14. Grimsley JK, Calamini B, Wild JR, Mesecar AD.Structural and mutational studies of organophosphorus hydrolase reveal a cryptic and functional allosteric-binding site. *Arch Biochem Biophys* 2005;442:169–79.
15. Jackson CJ, Carr PD, Kim HK, Liu JW, Herrald P, Mitic N, Schenk G, Smith CA, Ollis DL.Anomalous scattering analysis of Agrobacterium radiobacter phosphotriesterase: the prominent role of iron in the heterobinuclear active site. *Biochem J* 2006;397:501–8.
16. Rochu D, Beaufet N, Renault F, Viguie N, Masson P.The wild type bacterial Co(2+)/Co(2+)-phosphotriesterase shows a middle-range thermostability. *Biochim Biophys Acta* 2002;1594:207–18.
17. Serdar C, Murdock DC, Rohde MF.Parathion hydrolase gene from Pseudomonas diminuta MG: subcloning, complete nucleotide sequence, and expression of the mature protein of the enzyme in E. coli. *Biotechnol.* 1989;7:1151–55.

18. Hartl DL, Ochman H.Inverse polymerase chain reaction. *Methods Mol Biol* 1996;58:293–301.
19. Briseno-Roa L, Hill J, Notman S, Sellers D, Smith AP, Timperley CM, Wetherell J, Williams NH, Williams GR, Fersht AR, Griffiths AD.Analogues with fluorescent leaving groups for screening and selection of enzymes that efficiently hydrolyze organophosphorus nerve agents. *J Med Chem* 2006;49:246–55.
20. Dumas DP, Caldwell SR, Wild JR, Raushel FM.Purification and properties of the phosphotriesterase from Pseudomonas diminuta. *J Biol Chem* 1989;264:19659–65.
21. Buchbinder JL, Stephenson RC, Dresser MJ, Pitera JW, Scanlan TS, Fletterick RJ.Biochemical characterization and crystallographic structure of an Escherichia coli protein from the phosphotriesterase gene family. *Biochemistry* 1998;37:5096–106.
22. Mulbry WW, Karns JS.Purification and characterization of three parathion hydrolases from gram-negative bacterial strains. *Appl Environ Microbiol* 1989;55:289–93.
23. Grimsley JK, Scholtz JM, Pace CN, Wild JR.Organophosphorus hydrolase is a remarkably stable enzyme that unfolds through a homodimeric intermediate. *Biochemistry* 1997;36:14366–74.
24. Benning MM, Shim H, Raushel FM, Holden HM.High resolution X-ray structures of different metal-substituted forms of phosphotriesterase from Pseudomonas diminuta. *Biochemistry* 2001;40:2712–22.
25. Dong YJ, Bartlam M, Sun L, Zhou YF, Zhang ZP, Zhang CG, Rao Z, Zhang XE.Crystal structure of methyl parathion hydrolase from Pseudomonas sp. WBC-3. *J Mol Biol* 2005;353:655–63.
26. Watkins LM, Mahoney HJ, McCulloch JK, Raushel FM.Augmented hydrolysis of diisopropyl fluorophosphate in engineered mutants of phosphotriesterase. *J Biol Chem* 1997;272:25596–601.
27. Roodveldt C, Tawfik DS.Directed evolution of phosphotriesterase from Pseudomonas diminuta for heterologous expression in Escherichia coli results in stabilization of the metal-free state. *Protein Eng Des Sel* 2005;18:51–8.
28. Volkman BF, Lipson D, Wemmer DE, Kern D.Two-state allosteric behavior in a single-domain signaling protein. *Science* 2001;291:2429–33.
29. Bahar I, Chennubhotla C, Tobi D.Intrinsic dynamics of enzymes in the unbound state and relation to allosteric regulation. *Curr Opin Struct Biol* 2007;17:1–8.
30. Kuo JM, Raushel FM.Identification of the histidine ligands to the binuclear metal center of phosphotriesterase by site-directed mutagenesis. *Biochemistry* 1994;33:4265–72.
31. Mee-Hie Cho C, Mulchandani A, Chen W.Functional analysis of organophosphorus hydrolase variants with high degradation activity towards organophosphate pesticides. *Protein Eng Des Sel* 2006;19:99–105.
32. Yang H, Carr PD, McLoughlin SY, Liu JW, Horne I, Qiu X, Jeffries CM, Russell RJ, Oakeshott JG, Ollis DL.Evolution of an organophosphate-degrading enzyme: a comparison of natural and directed evolution. *Protein Eng* 2003;16:135–45.